

Participation Ratio as a Quantum Probe of Hierarchical Stickiness

Ariel A. Galindo Duque,^{1,*} Miguel A. Prado Reynoso,^{1,2,†} Miguel Gonzalez,^{1,3,‡} and Jorge G. Hirsch,^{1,§}

¹*Instituto de Ciencias Nucleares, Instituto de Ciencias Nucleares, Universidad Nacional Autónoma de México, Apdo. Postal 70-543, C.P. 04510 Cd. Mx., Mexico*

²*Nonlinear Dynamics, Chaos and Complex Systems Group, Departamento de Física, Universidad Rey Juan Carlos, Tulipán s/n, 28933 Móstoles, Madrid, Spain*

³*Center for Theoretical Physics of Complex Systems, Institute for Basic Science (IBS), Daejeon 34126, Republic of Korea*

We investigate how quantum localization encodes the hierarchical stickiness that governs transport in mixed classical phase spaces. Using the periodically driven kicked top, we show that the participation ratio (PR) of coherent states in the Floquet eigenbasis resolves the same layered structure that appears classically as a multimodal distribution of finite-time Lyapunov exponents (FTLEs). To establish a quantitative correspondence, we introduce a Gaussian coarse graining of the FTLE matched to the intrinsic semiclassical resolution of coherent states. Both local correlations and global comparisons of probability distributions demonstrate that quantum and classical indicators agree optimally within a finite window of evolution times, where sticky structures are most clearly resolved. Our results promote the participation ratio from a global measure of chaos to a sensitive probe of hierarchical transport and provide a practical route for diagnosing anomalous localization in driven quantum systems.

I. INTRODUCTION

Understanding how classical phase-space structures manifest themselves in quantum dynamics remains a central problem of quantum chaos. In systems with mixed phase space, remnants of invariant tori and partial transport barriers organize chaotic transport and generate long trapping times, a phenomenon commonly known as stickiness. [1–4].

The participation ratio (PR) has become a standard observable to quantify quantum-state delocalization and to discriminate between regular and chaotic regimes [1, 5–7]. In mixed systems it has been successfully used to separate regular from chaotic eigenstates [1, 5–8]. Here we demonstrate that the PR contains substantially finer information: it resolves the hierarchical organization of the chaotic sea itself.

Classically, stickiness [9–17] is efficiently characterized through finite-time Lyapunov exponents (FTLEs). Rather than forming a single chaotic component, FTLE distributions typically display multiple modes associated with nested layers of instability [18–29]. Whether and how this hierarchy is encoded in quantum observables remains largely unexplored.

Periodically driven systems with a clear classical limit provide an ideal setting for addressing this question [30, 31]. Among them, the kicked top offers a paradigmatic framework in which coherent states furnish localized semiclassical probes while quantum evolution is governed by a well-defined Floquet operator [8, 32–35].

In this work we analyze coherent states expanded in the Floquet eigenbasis and show that their participation

ratio reproduces the multimodal structure of the classical FTLE distribution. To make the correspondence quantitative, we introduce a Gaussian coarse graining of the FTLE matched to the intrinsic semiclassical resolution of coherent states. Using both pointwise and distributional measures, we identify an optimal time window in which classical hierarchical structures are most faithfully encoded in quantum localization.

Our results promote the participation ratio from a global indicator of chaos to a sensitive probe of hierarchical transport and provide a practical diagnostic of anomalous localization in driven quantum systems.

The paper is organized as follows. In Sec. II, we introduce the classical and quantum kicked top, define the effective Planck constant, and construct coherent states on the sphere. In Sec. III, we introduce the participation ratio in the Floquet basis and discuss its role as a global indicator of the regular–chaotic transition. Section IV analyzes classical stickiness through finite-time Lyapunov exponents and demonstrates how quantum stickiness emerges in participation-ratio distributions. Section V examines the dependence of PR–FTLE correlations on the FTLE time window and on \hbar_{eff} . Finally, Sec. VI summarizes our conclusions and discusses possible extensions to higher-dimensional and many-body systems.

II. REGULAR–CHAOTIC TRANSITION IN THE KICKED TOP MODEL

A. The kicked top model

The kicked top is a paradigmatic model for exploring chaotic dynamics in both classical and quantum mechanics. The quantum system is described by an angular momentum vector $\hbar\mathbf{J} = \hbar(\hat{J}_x, \hat{J}_y, \hat{J}_z)$, whose components satisfy the $SU(2)$ commutation relations $[\hat{J}_i, \hat{J}_j] =$

* ariel.galindo@ciencias.unam.mx

† miguelangel.prado@urjc.es

‡ miguel.gonzalez@correo.nucleares.unam.mx

§ hirsch@nucleares.unam.mx

$i\varepsilon_{ijk}\hat{J}_k$. In the setup we study, the system's dynamics are governed by the time-dependent Hamiltonian

$$\hat{H}(t) = \hbar\alpha\hat{J}_z + \frac{\hbar k}{2J}\hat{J}_x^2 \sum_{n=-\infty}^{\infty} \delta(t-n) \quad (1)$$

where the first term describes free precession around the z -axis with frequency α , while the second term represents periodic kicks applied along the x -axis. The period between successive kicks has been set to unity. Each kick induces an instantaneous rotation about the x -axis by an angle proportional to J_x , with the proportionality factor given by the dimensionless coupling constant k . By applying Floquet's theorem, we can describe the evolution of the system in terms of the one-period evolution operator

$$\hat{U} = \exp(-i\alpha\hat{J}_z) \exp\left(-\frac{ik}{2J}\hat{J}_x^2\right) \quad (2)$$

where we set $\hbar = 1$. The squared angular momentum operator, \hat{J}^2 , is a conserved quantity satisfying $[\hat{J}^2, \hat{H}(t)] = 0$ and $[\hat{J}^2, \hat{U}] = 0$, with eigenvalues $J(J+1)$. As a result, one can describe the dynamics at a fixed value of J .

The $(2J+1)$ -dimensional Hilbert space is spanned by the simultaneous eigenstates of \hat{J}^2 and \hat{J}_z , the well-known Dicke base. The spectral decomposition of the operator (2), $\hat{U}|\phi_j\rangle = e^{i\phi_j}|\phi_j\rangle$, yields the $(2J+1)$ Floquet eigenstates $|\phi_j\rangle$ and their corresponding quasi-energies ϕ_j .

The classical Hamiltonian can be obtained from the quantum Hamiltonian (1) by taking the expectation value with respect to spin-coherent [36] states, as explained in Appendix A:

$$H = \alpha J_z + \frac{k}{2} J_x^2 \sum_{n=-\infty}^{\infty} \delta(t-n) \quad (3)$$

The parameter k controls the strength of the kicks and acts as the nonlinearity parameter of the system.

By integrating Hamilton's equations of (A2) over one period, we can obtain the stroboscopic evolution of the system, described by the iterated map

$$\begin{aligned} J_{n+1}^x &= \cos\alpha J_n^x - \sin\alpha [J_n^y \cos(kJ_n^x) + J_n^z \sin(kJ_n^x)] \\ J_{n+1}^y &= \sin\alpha J_n^x + \cos\alpha [J_n^y \cos(kJ_n^x) - J_n^z \sin(kJ_n^x)] \\ J_{n+1}^z &= J_n^y \sin(kJ_n^x) + J_n^z \cos(kJ_n^x) \end{aligned} \quad (4)$$

B. The participation ratio as a quantum signal of chaos

The participation ratio (PR) is a standard measure of quantum-state localization in a chosen basis and is directly connected to the second-order Rényi entropy [37–39].

For a pure state $|\psi\rangle$ expanded in an orthonormal basis $\{|\phi_j\rangle\}_{j=1}^N$ of dimension N , we define the *normalized participation ratio* as

$$PR = \frac{1}{N} \left(\sum_{j=1}^N |\langle\phi_j|\psi\rangle|^4 \right)^{-1}, \quad (5)$$

which takes values in the interval $PR \in [1/N, 1]$, corresponding to complete localization on a single basis state and uniform delocalization over the full Hilbert space, respectively.

We evaluate this quantity for spin coherent states [Eq. (A4)], expressed in the Floquet eigenbasis of the kicked-top evolution operator [Eq. (2)]. By construction, the normalized participation ratio probes the local degree of delocalization of semiclassical states in phase space, providing a direct quantum signature of the underlying classical dynamics.

Its use as a quantum indicator of the regular–chaotic transition is by now well established and has been extensively explored in a wide variety of quantum systems (see, e.g., Refs. [1, 5–7]). In these studies, the PR has been shown to reliably distinguish between regular and chaotic regimes through systematic changes in the degree of localization of quantum states, as well as through its sensitivity to fixed points and unstable periodic orbits (UPOs) [40–42].

In Appendix B a detailed analysis of the regular–chaotic transition is presented. This transition is consistently captured by three complementary indicators: the classical chaotic area fraction μ_k , the quantum quasienergy level-spacing statistic r , and the phase space averaged participation ratio $\langle PR \rangle$. The latter captures the same transition through the localization properties of coherent states, without relying on spectral statistics.

III. CLASSICAL AND QUANTUM MANIFESTATIONS OF HIERARCHICAL STICKINESS

In the present work we explore the phenomenon of stickiness within the mixed regime, concentrating on the representative case of a kicking strength $k = 3.0$. We fix $\alpha = 0.84$.

Mixed phase spaces exhibit a hierarchical organization in which chaotic trajectories may remain trapped near remnants of invariant tori for extended times. This stickiness leads to anomalous transport and is reflected in the statistics of finite-time Lyapunov exponents (FTLEs). We show that the same hierarchical structure is resolved by the participation ratio (PR) of coherent states in the Floquet eigenbasis.

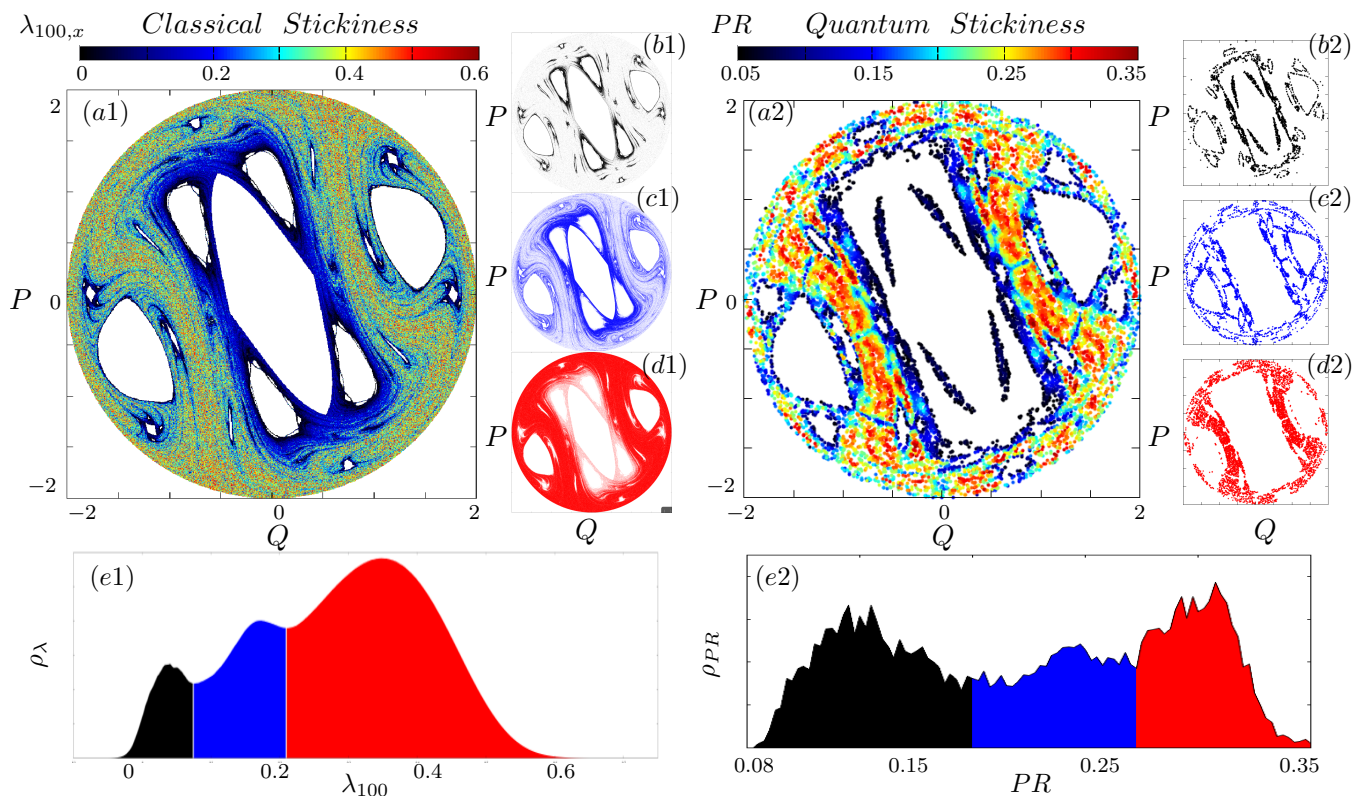


FIG. 1. Hierarchical stickiness in the kicked top for $k = 3$. (a1) Finite-time Lyapunov exponent (FTLE) distribution over the chaotic sea in classical phase space. (b1–d1) Phase space partitioned according to intervals of FTLE values. (e1) Multimodal histogram of the FTLE density. (a2) Distribution of the participation ratio (PR) of coherent states in phase space for $J = 500$. (b2–d2) Phase space partitioned according to intervals of PR values. (e2) Multimodal histogram of the PR density.

A. Classical hierarchy from finite-time Lyapunov exponents

For each initial condition, we compute the finite-time Lyapunov exponent (FTLE), defined in Appendix C, over different evolution times. In a uniformly hyperbolic system, the FTLE distribution is unimodal. In contrast, mixed systems exhibit a multimodal structure: distinct peaks correspond to regions with different instability levels.

Figure 1(a1) shows the phase-space distribution of the FTLE. The chaotic sea does not form a homogeneous component; instead, it is organized in layers surrounding regular islands. These layers are associated with progressively smaller Lyapunov exponents, indicating increasingly long trapping times. They are shown individually in Figs 1(b1, c1, d1).

The corresponding FTLE distribution [Fig. 1(e1)] displays multiple peaks. The largest exponent corresponds to strongly chaotic trajectories, while secondary peaks arise from sticky regions near partial transport barriers. This multimodality provides a quantitative fingerprint of hierarchical stickiness.

B. Quantum signatures of stickiness in the Participation Ratio

To probe the quantum dynamics locally in phase space, we expand coherent states in the Floquet eigenbasis and compute their participation ratio.

Figure 1(a2) shows the PR mapped over phase space. Regular islands are not colored. Within the chaotic sea the PR is not uniform: it exhibits structured variations mirroring the classical hierarchy. The individual layers are shown in Figs. 1(b2, c2, d2).

The PR distribution [Fig. 1(e2)] reveals multiple peaks analogous to those of the FTLE distribution. Regions corresponding to smaller classical Lyapunov exponents are associated with reduced quantum delocalization. Thus, the PR resolves not only the regular–chaotic transition but also the layered structure inside the chaotic component.

This correspondence indicates that quantum localization encodes classical transport barriers beyond the global distinction between order and chaos.

IV. QUANTITATIVE QUANTUM–CLASSICAL CORRESPONDENCE

The qualitative agreement between FTLE and PR phase-space maps suggests a deeper quantitative relationship. We now compare classical instability and quantum delocalization using both local correlations and global distributional measures.

A. Resolution matching and Gaussian coarse graining

A direct comparison between FTLE and PR requires accounting for their different phase-space resolutions. Classical trajectories probe arbitrarily fine structures, whereas coherent states provide a finite semiclassical resolution set by $\hbar_{\text{eff}} = 1/J$.

To establish a consistent comparison, we introduce a Gaussian coarse graining of the FTLE field (GFTLE), as explained in Appendix D. The width is chosen to match the intrinsic spread of coherent states. This procedure filters classical structures below quantum resolution while preserving the hierarchical organization.

Figures 2(a, b, c) show the coarse-grained GFTLE map for three different times: $\tau = 1, 100$ and 5000 , while Figs 2(d, e, f) display the PR distribution for $J = 500, 1000$ and 1500 , illustrating the enhanced resolution of classical phase-space structures as $\hbar_{\text{eff}} \sim J^{-1}$ decreases.

It can be seen that the GFTLE map for $\tau = 100$ closely resembles the PR landscape, including the layered structure within the chaotic sea.

B. Local correlation analysis

We quantify the pointwise correspondence using the Pearson correlation coefficient between the PR and the GFTLE. Given two data sets

$$A = \{A_i\}, \quad B = \{B_i\},$$

evaluated at identical phase-space points (Q_i, P_i) , we define the Pearson correlation coefficient as

$$C_p = \frac{\text{Cov}(A, B)}{\sigma_A \sigma_B}, \quad (6)$$

where $\text{Cov}(A, B)$ denotes the covariance between A and B , and σ_A, σ_B are their respective standard deviations.

Figure 2(g) shows the correlation as a function of evolution time τ . The agreement is not monotonic: correlations increase for intermediate times and decrease for both short and long times. Short times do not resolve transport barriers, while long times smear hierarchical distinctions. An optimal time window emerges in which classical and quantum indicators are maximally aligned.

The dependence on spin size J [Fig.2(g)] confirms the semiclassical origin of the correspondence. Increasing J

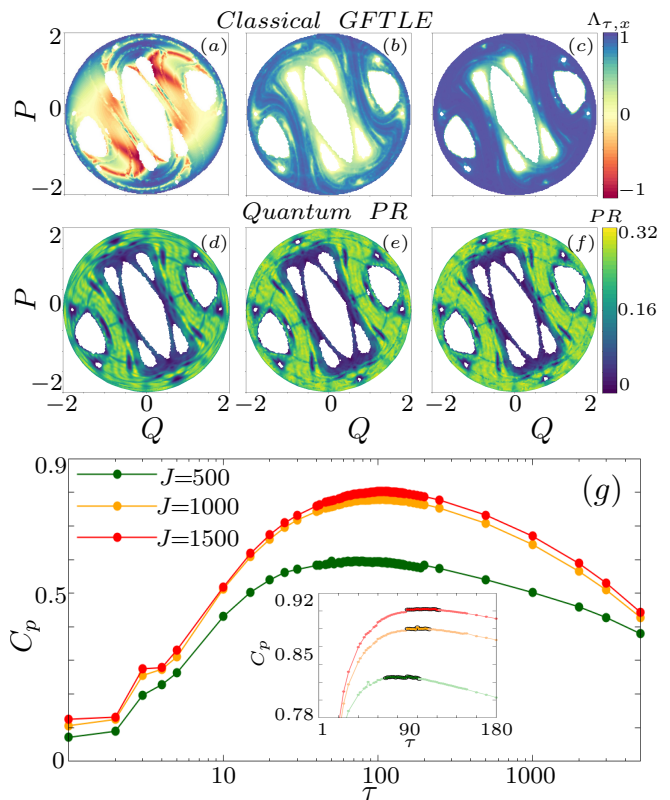


FIG. 2. (a)-(c) GFTLE distribution using a Gaussian smoothing width $\sigma^2 = 1/J$ for time windows $\tau = 1, 100$, and 5000 . (d)-(f) PR distribution of coherent states for $J = 500, 1000$, and 1500 . (g) Pearson correlation coefficient between the GFTLE and the PR.

enhances resolution and sharpens correlations, consistent with the expectation that quantum localization increasingly reflects classical structures as $\hbar_{\text{eff}} \rightarrow 0$.

C. Comparison of distributions

In Figs. 3(a)-(c), we plot the histogram of the density Gaussian-smoothed finite-time Lyapunov exponent (GFTLE) for three different time windows, $\tau = 1, 100$, and 5000 , respectively. Figures 2(d)-(f) display the quantum counterpart, the histogram of the PR density for three different values of the spin magnitude, $J = 500, 1000$, and 1500 .

We observe that the distribution of the Gaussian-smoothed FTLE shown in Fig.3(a) differs slightly from the FTLE distribution in Fig. 2(a). This difference is not solely due to the coarse graining introduced by the Gaussian smoothing, but also to the way the distributions are sampled. The FTLE distribution in Fig. 2(a) is computed with respect to the natural (Sinai–Bowen–Ruelle)[43–45] measure induced by the dynamics, whereas the GFTLE distribution is obtained by sampling uniformly over phase space. This uniform sampling is consistently used for the computation of all GFTLE and PR distributions, ensur-

ing a fair comparison between the classical and quantum indicators.

D. Distributional correlation between PR and GFTLE

Beyond pointwise correlations, we compare the full probability distributions of PR and coarse-grained FTLE values. The Jensen–Shannon distance provides a symmetric measure of similarity between distributions.

Let $F = \{f_k\}$ and $G = \{g_k\}$ denote two normalized histograms defined over a common support. We introduce the mixed distribution $M = (F + G)/2$, with components $m_k = (f_k + g_k)/2$. The Jensen Shannon divergence between F and G is defined as

$$\text{JSD}(F|G) = \frac{1}{2}D_{\text{KL}}(F|M) + \frac{1}{2}D_{\text{KL}}(G|M), \quad (7)$$

where

$$D_{\text{KL}}(F|M) = \sum_k f_k \ln \left(\frac{f_k}{m_k} \right)$$

is the Kullback–Leibler divergence. The corresponding Jensen–Shannon distance is

$$D_{\text{JS}}(F, G) = \sqrt{\text{JSD}(F|G)}, \quad (8)$$

which satisfies $0 \leq D_{\text{JS}}(F, G) \leq \sqrt{\ln 2}$.

This metric provides a global statistical comparison between the quantum and classical indicators, revealing how closely the hierarchical structures encoded in their distributions align.

In agreement with the Pearson correlation analysis, we find that the smallest Jensen Shannon distances between classical and quantum indicators are located at intermediate time windows, approximately in the range $\tau \simeq 50$ – 120 . Outside this range, the Jensen Shannon distance increases, indicating that the PR distributions are either unable to resolve the relevant hierarchical structures at short times or become overly smoothed at long times. [32, 33]).

J	t_{JS}	$t_{\rho_{XY}}$
500	(50:92)	(68:100)
1000	(56:102)	(90:110)
1500	(66:94)	(90:120)

TABLE I. Time windows $t_{\rho_{XY}}$, around the maximum of the Pearson correlation, and t_{JS} , around the minimum of the Jensen Shannon distance, for three values of J .

Table I shows the time windows at which the Jensen–Shannon distance reaches its minimum and the Pearson correlation coefficient reaches its maximum for the three spin magnitudes considered: $J = 500, 1000$, and 1500 . The existence of an optimal time window where both measures coincide reflects a competition between barrier resolution and ergodic averaging.

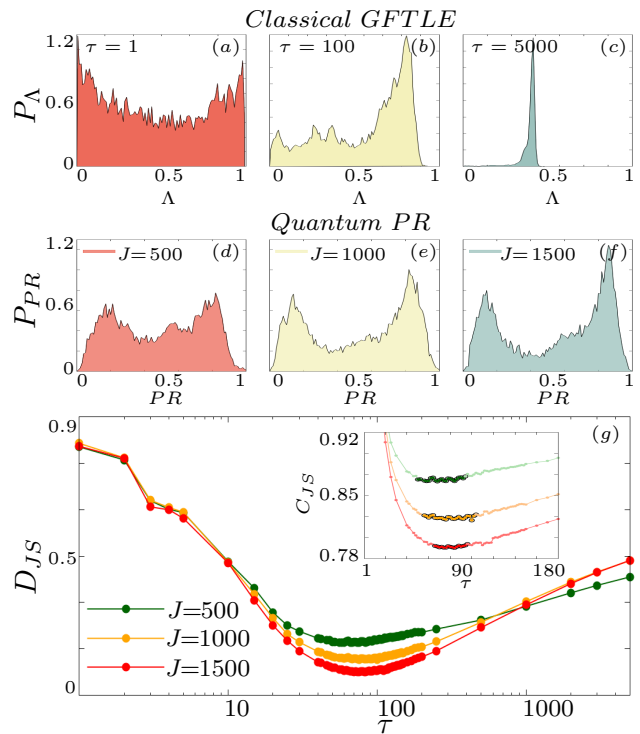


FIG. 3. (a)-(c) GFTLE probability distributions for $\tau = 1, 100$, and 5000 . (d)-(f) PR probability distributions for $J = 500, 1000$, and 1500 . (g) Jensen–Shannon distance between the GFTLE and PR as a function of the time window τ (logarithmic scale). Inset: magnified view of the region around the minimum, in linear scale.

V. SUMMARY AND CONCLUSIONS

We have shown that hierarchical stickiness in mixed phase space is quantitatively encoded in quantum localization. The participation ratio of coherent states does not merely distinguish regular from chaotic regions; it resolves the layered structure within the chaotic sea that arises from partial transport barriers.

By introducing a Gaussian coarse graining of the finite-time Lyapunov exponent, matched to the intrinsic semiclassical resolution of coherent states, we established a direct quantum–classical correspondence. The agreement is maximized within an intermediate evolution-time window, reflecting a competition between two mechanisms: short times fail to resolve hierarchical trapping, whereas long times average over it. This optimal window identifies the temporal scale at which classical transport structures are most faithfully imprinted onto quantum eigenstates.

The dependence of the correlation on spin size confirms the semiclassical origin of this effect: as $\hbar_{\text{eff}} \rightarrow 0$, quantum localization increasingly mirrors the classical hierarchy. The correspondence is therefore not incidental but structurally rooted in the phase-space organization of mixed systems.

Our results demonstrate that participation ratios pro-

vide a local diagnostic of classical transport barriers beyond the global regular–chaotic transition. This framework can be extended to other Floquet systems and to higher-dimensional or many-body settings where hierarchical transport structures play a central role.

ACKNOWLEDGMENTS

We acknowledge the support of the Computation Center - ICN to develop many of the results presented in this work, in particular to Enrique Palacios, Luciano Díaz, and Eduardo Murrieta. This work received partial financial support from DGAPA- UNAM projects IN109523 and IN101526.

AUTHOR DECLARATIONS

Conflict of Interest

The authors have no conflicts to disclose.

Author Contributions

Ariel A. Galindo Duque: Conceptualization (equal); Investigation (equal); Methodology (equal); Software (equal); Writing – review (equal). **Miguel A. Prado Reynoso:** Conceptualization (equal); Methodology (equal); Supervision (supporting); Writing – original draft (lead). **Miguel Gonzalez:** Conceptualization (supporting); Methodology (equal); Software (equal); Writing – review (equal). **Jorge G. Hirsch:** Supervision (lead); Conceptualization (equal); Formal analysis (equal); Methodology (equal); Writing – review and editing (lead).

Appendix A: Classical and quantum kicked top

The quantum kicked top is defined by the Floquet operator (2). To probe the quantum dynamics locally in phase space, we employ spin-coherent states

$$|\theta, \phi\rangle = e^{i\theta(\hat{J}_y \sin \phi - \hat{J}_x \cos \phi)} |J, J\rangle, \quad (\text{A1})$$

which are minimal-uncertainty states over the surface of the Bloch sphere centered at the point (θ, ϕ) . Their resolution scales as $\Delta\theta \approx \Delta\phi \approx J^{-1/2}$.

Taking the expectation value of the angular momentum operators with respect to spin-coherent states allows to introduce the classical variables

$$\lim_{J \rightarrow \infty} \langle \theta, \phi | \hat{\mathbf{J}} | \theta, \phi \rangle = \vec{J} = (J_x, J_y, J_z).$$

The classical Hamiltonian is obtained from the quantum Hamiltonian (1) by taking the expectation value

with respect to spin-coherent [36] states and then taking the limit $J \rightarrow \infty$, as follows:

$$H = \lim_{J \rightarrow \infty} \left\{ \frac{\langle \hat{H}(t) \rangle_{\theta, \phi}}{J} \right\} = \alpha J_z + \frac{k}{2} J_x^2 \sum_{n=-\infty}^{\infty} \delta(t-n) \quad (\text{A2})$$

We parametrize the classical spherical phase space \mathbf{S}_2 by its stereographic coordinates

$$Q = \frac{\sqrt{2}J_x}{\sqrt{1-J_z}}, \quad P = \frac{\sqrt{2}J_y}{\sqrt{1-J_z}}, \quad (\text{A3})$$

where the projection sends the sphere onto the disk $Q^2 + P^2 < 4$. Using this parametrization, the associated spin coherent state takes the form

$$|z(Q, P)\rangle = \frac{e^{z\hat{J}_+}}{(1+|z|)^J} |J, -J\rangle \quad (\text{A4})$$

where $z = (Q + iP)/\sqrt{4 - (Q^2 + P^2)}$ and $\hat{J}_+ = \hat{J}_x + i\hat{J}_y$ is the creation operator.

Appendix B: Participation Ratio Across the Regular–Chaotic Transition

In this section we analyze the regular-chaotic transition by jointly examining the evolution of classical phase space structures and their quantum counterparts as the kicking strength k is varied, while keeping the value $\alpha = 0.84$ fixed. This transition is consistently captured by three complementary indicators: the classical chaotic area fraction μ_k , the quantum quasienergy level-spacing statistic r , and the phase space averaged participation ratio $\langle PR \rangle$. The latter captures the same transition through the localization properties of coherent states, without relying on spectral statistics. These indicators are shown in Figs. 4(g), 4(h), and 4(i), respectively.

For each value of k , we generate 1000 random initial conditions and compute the Lyapunov spectrum over an evolution time of $t = 10^6$. For the quantum calculations, we present results for two angular momentum magnitudes: $J = 500$ and $J = 1500$. It can be seen that both values provide a well-defined semiclassical regime.

At weak kicking strengths, $k \lesssim 2.5$, the dynamics remain predominantly regular. Phase space is largely filled with invariant tori and stable periodic orbits, as illustrated in Fig. 4(a), and the chaotic fraction μ_k is close to zero. In this regime, the quasienergy spectrum exhibits Poisson-like statistics, reflected by small values of the level-spacing parameter r , while the phase-space-averaged participation ratio remains low. Consistently, the corresponding PR landscapes display strongly localized coherent states, indicating the persistence of classical regularity in the quantum dynamics (see Fig. 4(d)). Notice that the largest value of the PR is very small: 0.04).

As k increases into the intermediate range $2.5 \lesssim k \lesssim 4$, the system enters a mixed dynamical regime in which

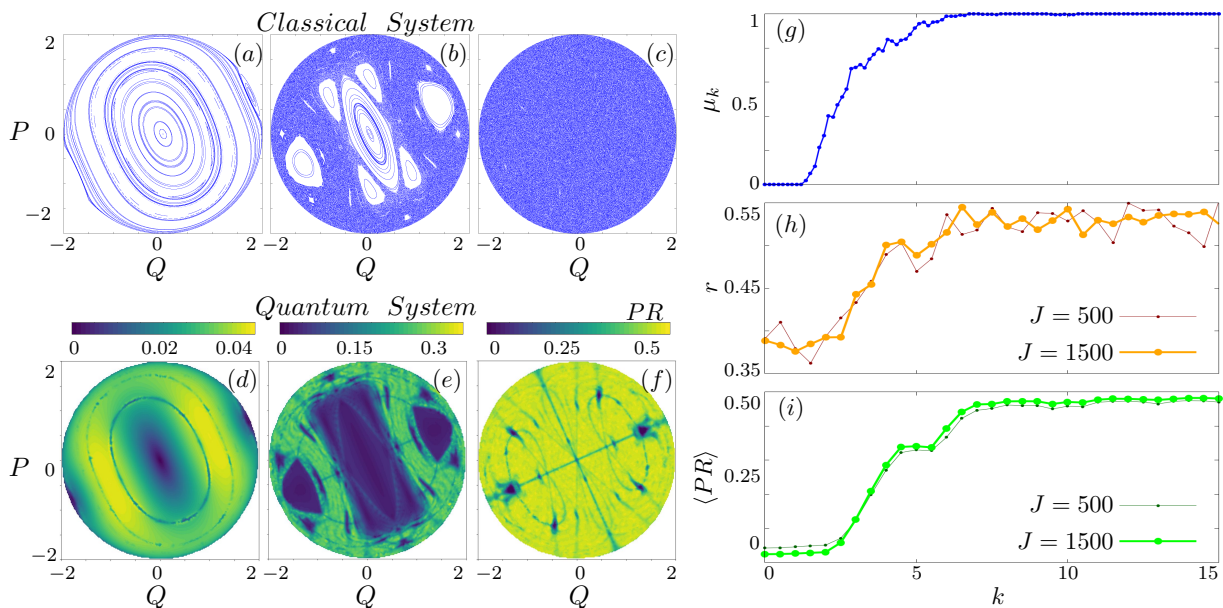


FIG. 4. (a–c) Classical phase space for increasing kick strength $k = 1, 4$, and 10 , showing the progressive destruction of invariant tori and the growth of the chaotic sea. (d–f) Quantum counterparts obtained from the participation ratio of coherent states evaluated over phase space for the same parameter values. (g) Fraction of chaotic phase-space area relative to the regular region as a function of the kick strength. (h) Level-spacing parameter characterizing the spectral transition from regular to chaotic statistics. (i) Phase-space-averaged participation ratio as a function of the kick strength.

regular islands coexist with chaotic layers, as shown in Fig. 4(b). The breakup of separatrices leads to heteroclinic and homoclinic tangles, generating a hierarchical organization of phase space and long-lived trapping of chaotic trajectories in sticky regions [39, 46]. In this regime, the chaotic area fraction μ_k grows steadily, while the level-spacing statistic r departs from Poisson behavior but has not yet reached its fully chaotic limit. At the same time, the average participation ratio increases, and the PR landscapes exhibit intermediate values, signaling partial delocalization of coherent states. As discussed in the following section, this behavior constitutes a clear quantum manifestation of classical stickiness (see Fig. 4(e)).

For sufficiently strong kicking, $k > 4$, the dynamics become globally chaotic, with phase space almost entirely covered by chaotic trajectories, as illustrated in Fig. 4(c). Only small stability islands survive, and their phase-space measure rapidly approaches zero, leading to saturation of the chaotic fraction μ_k . In this regime, the level-spacing statistic r approaches the predictions of random-matrix theory, and the phase-space-averaged participation ratio attains uniformly high values. Accordingly, coherent states are almost completely delocalized over the Floquet eigenbasis, and the PR is nearly uniform throughout phase space (see Fig. 4(f)).

Notably, this near-uniformity is punctuated by a set of thin, curve-like structures along which the PR attains values that are slightly lower than the typical values observed in this regime. Although the PR remains high overall, these filaments stand out against the otherwise

homogeneous background and signal localized deviations from complete delocalization. While their detailed origin and dynamical significance are not addressed here, their visibility suggests the persistence of correlations and symmetries in phase space. A dedicated analysis of these low-PR curves will be presented in future work.

Appendix C: Lyapunov exponents

For an invertible, measure-preserving map $f : M \rightarrow M$, the asymptotic Lyapunov exponent associated with an initial condition \mathbf{x} and tangent vector \mathbf{u} is defined as

$$\lambda = \lim_{t \rightarrow \infty} \frac{1}{t} \log \|D_{\mathbf{x}} f^t(\mathbf{u})\|, \quad (\text{C1})$$

where $\lambda > 0$ signals chaotic behavior.

The FTLE measures the local divergence rate of nearby trajectories over a finite time window, it is particularly sensitive to sticky dynamics: trajectories that linger near regular islands exhibit temporarily reduced instability, resulting in anomalously small FTLE values. Spatial variations of the FTLE therefore provide a natural diagnostic of the hierarchical structures that surround regular islands in mixed phase space.

The FTLE follows directly from the invariance of the unstable tangent space underlying the asymptotic Lyapunov exponent introduced in Eq. (C1). For a unit tangent vector $v_{\mathbf{x}}^u$ aligned with the corresponding unstable direction, the FTLE associated with the trajectory

$\{f^\tau(\mathbf{x})\}$ of time τ , is defined as

$$\lambda_{\tau,\mathbf{x}} = \frac{1}{\tau} \log \|D_{\mathbf{x}} f^\tau(v_{\mathbf{x}}^u)\|. \quad (\text{C2})$$

In the limit $\tau \rightarrow \infty$, the *FTLE* converges to the corresponding asymptotic Lyapunov exponent. In strictly regular regions, however, no unstable direction exists; consequently, the FTLE is not defined there.

Appendix D: Gaussian-smoothed finite time Lyapunov exponent (GFTLE).

Let $\lambda_{\tau,z}$ denote the FTLE evaluated at the point $z = (\theta, \varphi) \in \mathbb{S}^2$. For a reference point $x = (\theta_0, \varphi_0)$ at which we wish to compute a local classical instability measure,

we define the Gaussian smoothed FTLE (GFTLE) as

$$\Lambda_{\tau,x} = \frac{\int_{\mathbb{S}^2} \lambda_{\tau,z} \exp\left[-\frac{\gamma(z,x)^2}{2\sigma^2}\right] d\Omega}{\int_{\mathbb{S}^2} \exp\left[-\frac{\gamma(z,x)^2}{2\sigma^2}\right] d\Omega}, \quad \sigma^2 = \frac{1}{J}. \quad (\text{D1})$$

Here $\gamma(z, x) = \arccos(\cos \theta \cos \theta_0 + \sin \theta \sin \theta_0 \cos(\varphi - \varphi_0))$ is the geodesic distance on \mathbb{S}^2 , and $d\Omega = \sin \theta d\theta d\varphi$ is the standard surface element. The choice $\sigma^2 = 1/J$ is consistent with the angular spread of spin coherent states and ensures that the classical coarse graining matches the intrinsic quantum resolution set by \hbar_{eff} .

Importantly, this smoothing is performed directly in the angular-momentum phase-space variables, i.e., on the spherical manifold \mathbb{S}^2 where the classical kicked-top dynamics is defined.

-
- [1] M. A. Bastarrachea-Magnani, B. López-del Carpio, J. Chávez-Carlos, S. Lerma-Hernández, and J. G. Hirsch, *Phys. Rev. E* **93**, 022215 (2016).
- [2] S. Pilatowsky-Cameo, D. Villaseñor, M. A. Bastarrachea-Magnani, S. Lerma-Hernández, F. Santos Lea, and J. G. Hirsch, *Quantum* **6**, 644 (2022).
- [3] N. Anand, G. Styliaris, M. Kumari, and P. Zanardi, *Phys. Rev. Res.* **3**, 023214 (2021).
- [4] M. A. P. Reynoso, E. M. Signor, S. D. Prado, and L. F. Santos, *Phys. Rev. E* **110**, L062201 (2024).
- [5] d. O. Wesley Florentino and P. Giancarlo Queiroz, *Phys. Rev. Res.* **37**, 3995 (2018).
- [6] L. M. Sieberer, T. Olsacher, A. Elben, M. Heyl, , P. Hauke, F. Haake, and P. Zoller, *Phys. Rev. Res.* **5**, 2056 (2019).
- [7] J. Chávez-Carlos, M. A. Prado Reynoso, R. G. Cortiñas, I. García-Mata, V. S. Batista, F. Pérez-Bernal, D. A. Wisniacki, and L. F. Santos, *Quantum Science and Technology* **10**, 015039 (2024).
- [8] Q. Wang and M. Robnik, *Phys. Rev. E* **107**, 054213 (2023).
- [9] G. Contopoulos, *Astron. J.* **76**, 147 (1971).
- [10] G. Contopoulos and M. Harsoula, *Int. J. Bifurc. Chaos* **18**, 2929 (2008).
- [11] G. Contopoulos and M. Harsoula, *Int. J. Bifurc. Chaos* **20**, 2005 (2010).
- [12] R. Dvorak, “Stickiness” in Dynamical Systems, in *The Dynamics of Small Bodies in the Solar System: A Major Key to Solar Systems Studies*, edited by B. A. Steves and A. E. Roy (Springer Netherlands, Dordrecht, 1999) pp. 509–534.
- [13] M. A. Prado Reynoso and M. W. Beims, *Communications in Nonlinear Science and Numerical Simulation* **110**, 106358 (2022).
- [14] M. A. P. Reynoso, R. M. da Silva, and M. W. Beims, *Chaos, Solitons & Fractals* **144**, 110640 (2021).
- [15] A. L. Livorati, M. S. Palmero, G. Díaz-I, C. P. Dettmann, I. L. Caldas, and E. D. Leonel, *Commun. Nonlinear Sci. Numer. Simul.* **55**, 225 (2018).
- [16] D. Borin, A. L. P. Livorati, and E. D. Leonel, *Chaos, Solitons & Fractals* **175**, 113965 (2023).
- [17] N. Voglis, P. Tsoutsis, and C. Efthymiopoulos, *Mon. Not. R. Astron. Soc* **373**, 280 (2006).
- [18] G. You and S. Leung, *J. of Comp. Phys.* **425**, 109905 (2021).
- [19] K. P. K. Stefański, K. Buszko, *Chaos* **20**, 033117 (2010).
- [20] E. H.-G. G. Drótos and C. López, *J. Phys. Complex* **2**, 025014 (2021).
- [21] A. Prasad and R. Ramaswamy, *Phys. Rev. E* **60**, 2761 (1999).
- [22] T. Manos and M. Robnik, *Phys. Rev. E* **91**, 042904 (2015).
- [23] M. A. Prado Reynoso, G. J. Delben, M. Schlesinger, and M. W. Beims, *Phys. Rev. E* **106**, L062201 (2022).
- [24] L. Storm, H. Linander, J. Bec, K. Gustavsson, and B. Mehlig, *Phys. Rev. Lett.* **132**, 057301 (2024).
- [25] E. Ott, *Chaos in Dynamical Systems* (Cambridge University Press, Cambridge, UK, 2002).
- [26] G. Lapeyre, *Chaos* **12**, 688 (2002).
- [27] M. R. Sales, M. Mugnaine, J. Szezech, R. L. Viana, N. M. Ibero Caldas, and J. Kurths, *Chaos* **33**, 033140 (2023).
- [28] M. A. Prado Reynoso and M. W. Beims, *Commun. Nonlinear Sci. Numer. Simul.* **110**, 106358 (2022).
- [29] S. C. Shadden, F. Lekien, and J. E. Marsden, *Physica D* **212**, 271 (2005).
- [30] F. L. Moore, J. C. Robinson, C. F. Bharucha, B. Sundaram, and M. G. Raizen, *Phys. Rev. Lett.* **75**, 4598 (1995).
- [31] S. Mudute-Ndumbe and E.-M. Graefe, *NJP* **22**, 103011 (2020).
- [32] A. Anand, J. Davis, and S. Ghose, *Phys. Rev. Res.* **6**, 023120 (2024).
- [33] Z. Zou and J. Wang, *Entropy* **24**, 1092 (2022).
- [34] V. M. Bastidas, P. Pérez-Fernández, M. Vogl, and T. Brandes, *Phys. Rev. Lett.* **112**, 140408 (2014).
- [35] S. Chaudhury, A. Smith, B. E. Anderson, S. Ghose, and P. S. Jessen, *Nature* **461**, 768–771 (2009).
- [36] H. Zhang and C. D. Batista, *Phys. Rev. B* **104**, 104409 (2021).
- [37] M. Gonzalez, M. A. Bastarrachea-Magnani, and J. G.

- Hirsch, *Phys. Rev. E* **112**, 024201 (2025).
- [38] M. A. Bastarrachea-Magnani, D. Villaseñor, J. Chávez-Carlos, S. Lerma-Hernández, L. F. Santos, and J. G. Hirsch, *Phys. Rev. E* **109**, 034202 (2024).
- [39] Q. Wang and M. Robnik, *Entropy* **23**, 1347 (2021).
- [40] S. Pilatowsky-Cameo, J. Chávez-Carlos, M. A. Bastarrachea-Magnani, P. Stránský, S. Lerma-Hernández, L. F. Santos, and J. G. Hirsch, *Phys. Rev. E* **101**, 010202 (2020).
- [41] S. Pilatowsky-Cameo, D. Villaseñor, M. A. Bastarrachea-Magnani, S. Lerma-Hernández, F. Santos Lea, and J. G. Hirsch, *Nature Communications* **12**, 852 (2021).
- [42] D. Villaseñor, S. Pilatowsky-Cameo, M. A. Bastarrachea-Magnani, S. Lerma-Hernández, and J. G. Hirsch, *Phys. Rev. E* **103**, 052214 (2021).
- [43] Y. G. Sinai, *Russian Mathematical Surveys* **27**, 21 (1972).
- [44] D. Ruelle, *American Journal of Mathematics* **98**, 619 (1976).
- [45] R. Bowen, *Springer* **470** (1975).
- [46] Q. Wang and F. Pérez-Bernal, *Phys. Rev. E* **104**, 034119 (2021).